Mechanisms of Self-Organization of Cortical Microtubules in Plants Revealed by Computational Simulations

Jun F. Allard,* Geoffrey O. Wasteneys,† and Eric N. Cytrynbaum*

*Institute of Applied Mathematics and †Department of Botany, University of British Columbia, Vancouver, British Columbia, Canada V6T 1Z2

Microtubules confined to the two-dimensional cortex of elongating plant cells must form a parallel yet dispersed array transverse to the elongation axis for proper cell wall expansion. Some of these microtubules exhibit free minus-ends, leading to migration at the cortex by hybrid treadmilling. Collisions between microtubules can result in plus-end entrainment ("zippering") or rapid depolymerization. Here, we present a computational model of cortical microtubule organization. We find that plus-end entrainment leads to self-organization of microtubules into parallel arrays, whereas catastrophe-inducing collisions do not. Catastrophe-inducing boundaries (e.g., upper and lower cross-walls) can tune the orientation of an ordered array to a direction transverse to elongation. We also find that changes in dynamic instability parameters, such as in *mor1-1* mutants, can impede self-organization, in agreement with experimental data. Increased entrainment, as seen in *clasp-1* mutants, conserves self-organization, but delays its onset and fails to demonstrate increased ordering. We find that branched nucleation at acute angles off existing microtubules results in distinctive sparse arrays and infer either that microtubule-independent or coparallel nucleation must dominate. Our simulations lead to several testable predictions, including the effects of reduced microtubule severing in katanin mutants.

INTRODUCTION

Microtubules (MTs) are ubiquitous biopolymers that endow animal cells with structural rigidity, intracellular transport, and the ability to proliferate. Without the constraints of an MT-organizing center, the MTs at the cortex of plant cells are able to self-organize into robust yet dynamic arrays. After cell division and disassembly of the phragmoplast array, MTs form de novo on the inside of the plasma membrane, where a strong association with the cell cortex forces their dynamics to play out on an effectively two-dimensional geometry (Wasteneys, 2002). Through polymer dynamics, interactions with the membrane and microtubule-associated proteins (MAPs), and MT–MT interaction, the thousands of MTs at the cortex (Dixit and Cyr, 2004) form a strikingly parallel array transverse to, but dispersed along, the cell's axis of elongation. This highly ordered transverse array can reform within 120 min of the initiation of MT assembly after drug-induced depolymerization (Wasteneys and Williamson, 1989a), and it is required to generate anisotropic mechanical properties of the cell wall, although the relationship between the cortical MT array and the oriented deposition of cellulose microfibrils is not yet clear (Himmelspach et al., 2003; Wasteneys, 2004; Wasteneys and Fujita, 2006). For recent reviews, see Wasteneys and Ambrose (2009), Ehrhardt

and Shaw (2006), Hashimoto and Kato (2006), and Wasteneys and Fujita (2006).

The study of MT organization in the absence of an MT-organizing center is important for understanding plant cell growth, but it also has implications for understanding acentrosomal MT organization in general. Systems for which organization relies on MT dynamics in concert with activity of MT cross-linking and bundling proteins have occurred in numerous contexts. These systems include mitotic spindle organization (Burbank et al., 2007; Groen et al., 2009), aster formation (Surrey et al., 2001; Pinot et al., 2009), and organelle positioning (Malikov et al., 2005).

MTs are stiff, polar polymers composed of tubulin. One end of the polymer, known as the plus-end, randomly switches between states of rapid growth and rapid shrinkage (Mitchison and Kirschner, 1984) as well as intermittent pauses (Shaw et al., 2003) in a phenomenon known as dynamic instability. Transitions from growth to shrinkage and shrinkage back to growth are known as catastrophe and rescue, respectively. The minus-end might remain static or can slowly depolymerize (Shaw et al., 2003). Although photobleaching studies show that individual tubulin subunits remain mostly fixed relative to the cell cortex (Shaw et al., 2003), this hybrid-treadmilling mechanism (dynamic instability at the plus-end and on-average shrinkage of the minus-end) allows individual MTs to migrate as the plus-end polymerizes (on average) and the minus-end depolymerizes.

The collision of two cortical MTs may result in several possible outcomes. If the angle of collision is steep, the incident MT may switch to the shrinking state, or it may continue to grow unperturbed, crossing over the barrier MT. If the angle of collision is shallow, the incident MT may become entrained with the barrier MT, after which the plus-end grows parallel to the barrier MT, resulting in a sharp bend in the MT at the site of collision. This phenomenon is

commonly referred to as "zippering" (Dixit and Cyr, 2004), but recently it has been suggested that this term should be reserved for situations in which two preformed MTs are progressively coaligned (Wasteneys and Ambrose, 2009). Here, we refer to this phenomenon as plus-end entrainment or, simply, entrainment. After an MT is entrained by another, the MTs form a bundle most likely mediated by members of the MAP65 class of MAPs, which cross-link adjacent MTs together with a spacing of 20–30 nm (Chan *et al.*, 1999). Once bundled, MTs remain dynamic (Shaw *et al.*, 2003), although possibly with different polymerization properties (Van Damme *et al.*, 2004). Other collision outcomes are possible: the incident MT may buckle before the barrier (Wightman and Turner, 2007); it may cross over the barrier and continue in a perturbed direction (Hashimoto and Kato, 2006); or, it may become severed at the cross-over point with the new MT formed from the leading end undergoing a gradual reorientation via treadmillling (Wightman and Turner, 2007).

In the absence of an organizing center, nucleation of new MTs occurs throughout the cortex. As in other eukaryotes, nucleation is mediated by the γ-tubulin ring complex (γ-TuRC) (Murata *et al.*, 2005). There is evidence that nucleation can occur in the absence of existing MTs (Wasteneys and Williamson, 1989b; Wasteneys *et al.*, 1993; Chan *et al.*, 2003) and also in an MT-dependent manner where γ-TuRC is distributed along extant MTs. New MTs have been reported to branch off extant MTs at a specific angle of 40° from (Wasteneys and Williamson, 1989b; Murata *et al.*, 2005) or parallel with (Wasteneys and Ambrose, 2009) the extant MTs. One hypothesis is that the minus-end of the new MT remains statically associated with the γ-TuRC for a short time until it is severed by the MT-severing protein katanin (Wasteneys, 2002; Murata *et al.*, 2005).

MOR1 is an MT-associated protein with the ability to alter several dynamic instability parameters, including increasing both shrinking and growing velocities. It is a homologue of XMAP215, which has MT polymerase activity in vitro (Brouhard *et al.*, 2008). Altering these parameters has a dramatic effect on the cortical MT array. The temperature-sensitive mutant *mor1-1* has an organized array at permissive temperature 21°C, whereas the dynamic instability parameters are modified significantly at 31°C and the MTs become short and disorganized (Whittington *et al.*, 2001; Kawamura and Wasteneys, 2008).

Strong association of cortical MTs to the cortex is essential for a properly organized array (Dhonukshe *et al.*, 2003; Ambrose and Wasteneys, 2008). Anchoring is believed to involve phospholipase D (Dhonukshe *et al.*, 2003) and the CLASP protein (Ambrose and Wasteneys, 2008). Inhibiting or perturbing either of these perturbs the MT array organization. In particular, in the *clasp-1* mutant in which *CLASP* transcripts are not present, anchor density is decreased and the distance between anchors is increased (Ambrose and Wasteneys, 2008). The free, unanchored length at the plus-end of a growing MT seems to entrain more readily in these mutants, as the free end can explore more space and be entrained with less curvature. Furthermore, the *clasp-1* mutant's array is more highly ordered (that is, with fewer deviations from the dominant orientation) than the wild-type array.

It has been widely hypothesized (Dixit and Cyr, 2004; Ehrhardt and Shaw, 2006; Wasteneys and Ambrose, 2009) that the MT–MT interactions outlined above can lead to the formation of an ordered array, where the majority of MTs point in the transverse direction relative to the major growth axis. However, this hypothesis remains to be tested theoretically. What MT–MT interactions are sufficient to lead to an organized array, and how long would this self-organization take to emerge? What are the relative importance of various aspects, such as the density and length of MTs? Computer simulations can address these questions in a way that experiments cannot. In a recent study simulating a similar system, by Baulin *et al.* (2007), a dominant direction indeed emerged. In their caricature of the plant system, each MT is constantly growing at one end and shrinking at the other end (at a slower rate) unless it encounters a barrier MT, in which case it pauses until the barrier MT has treadmilled out of its way. In a more closely related study by Dixit and Cyr (2004), simulations were carried out including collision-induced catastrophe (CIC) as well as plus-end entrainment (which they refer to as zippering). However, given the computational difficulty of the problem, the authors were only able to consider at most 20 MTs for 10 min, and a statistically meaningful interpretation is difficult to extract from their results.

Here, we present a computational study of cortical MTs in plants. We simulate several thousands of MTs over time scales of minutes to hundreds of minutes, including the effects of CIC, plus-end entrainment and MT-dependent nucleation. We explicitly model the *mor1-1* and the *clasp-1* mutants of *Arabidopsis thaliana* and find agreement with experiments for *mor1-1*, but not *clasp-1*. Our results illustrate assumptions under which an ordered array will emerge, and assumptions under which it does not.

MATERIALS AND METHODS

Ambrose and Wasteneys (2008) and Shaw *et al.* (2003) report cortical MTs switching spontaneously between growth (g), pause (p), and shrinkage (s). This three-state dynamic instability model thus involves eight parameters: six transition rates between the states f_{ij}, where $i,j = g,p,s$, and growth and shrinkage velocities v_g and v_s. As a simplification of this three-state model, a two-state dynamical instability model involving four parameters has been studied previously (Rubin, 1988; Dogterom and Leibler, 1993) and used extensively in cell biology (Grill and Hyman, 2005; Wollman *et al.*, 2005; Gardner *et al.*, 2008). The mean length (Dogterom and Leibler, 1993) and mean lifetime (Rubin, 1988) of an MT in the two-state model depend on a threshold quantity $f_{gs} v_s - f_{sg} v_g$. If the quantity is positive, the MTs tend to shrink more than they grow, and the MTs will have a finite mean length and mean lifetime. Otherwise, on average, they tend to grow forever. For the three-state case, we compute the equivalent equations in the Supplemental Material. There is an equivalent threshold quantity that determines if the MTs tend to remain finite or grow indefinitely. Note that these simplified models only consider dynamic instability: they are only valid in the absence of interactions between the MTs and any growth boundaries, and in the abundance of free tubulin. Thus, the mean length and mean lifetime should be thought of as characteristic scales that are perturbed by MT–MT interactions and the action of MAPs. Tables 1 and 2 summarize parameters from the literature (Shaw *et al.*, 2003; Dixit and Cyr, 2004; Kawamura and Wasteneys, 2008) that we use in this article.

We assume the minus-end is either always static, or continuously shrinking with constant rate v_s^m. Shaw *et al.* (2003) report MT minus-ends spending 25.3% of the time shrinking at, on average, 2.78 μm/min, and 8.4% of the time growing at 1.96 μm/min, and the remaining time (66.3%) paused. Thus, for instances in which we assume minus-ends shrink, we use an appropriately weighted average of these data: $v_s^m = 0.253$ (2.78 μm/min) + 0.084 (−1.96 μm/min) + 0.663 (0) = 0.53 μm/min.

When two MTs collide, the outcome depends on the angle between the incident and barrier MTs (Wasteneys and Ambrose, 2009), which we call the collision angle χ. We define the critical entrainment angle θ_Z as follows. If $\theta_X > \theta_Z$, the collision is steep and catastrophe occurs with probability p_{cat}, otherwise the incident MT crosses over the barrier MT (with probability $1 - p_{cat}$). In *A. thaliana*, 9% of steep-angle collisions result in catastrophe in petiole epidermal cells and 25% in leaf pavement cells (Wightman and Turner, 2007), whereas in tobacco BY2 cells, catastrophe results 60% of the time (Dixit and Cyr, 2004). In these studies, the angles 45° and 40°, respectively, were found to delineate the transition between entrainment and catastrophe.

If $\theta_X < \theta_Z$, the collision is shallow and plus-end entrainment occurs with probability p_{zip}. After an entrainment event, the extant segment of the incident MT remains in its precollision configuration, but the plus-end continues to grow parallel to the barrier MT. Thus, the MT is now composed of two line segments with a kink. In this article, we assume this phenomenological description of entrainment, neglecting fine-grain biophysical properties of the kink. The segment from the kink to the plus-end of the entrained MT is kept

Table 1. Dynamic instability parameters from three-state models using data from Kawamura and Wasteneys (2008) for wild type (WT) and the *mor1-1* mutant and Shaw *et al.*(2003), and two-state models using data from Dixit and Cyr (2004)

	WT[a] 21°C	WT[a] 31°C	mor1-1 21°C	mor1-1 31°C	Shaw et al. (2003)	Dixit and Cyr (2004)
Kawamura and Wasteneys						
f_{gp}	0.20	0.380	0.200	0.960	0.47	
f_{gs}	0.17	1.590	0.380	0.820	0.97	1.61
f_{pg}	2.01	1.400	1.560	0.700	0.51	
f_{ps}	1.02	0.700	0.560	0.620	0.24	
f_{sg}	1.00	1.990	1.180	0.610	0.87	3.26
f_{sp}	0.31	0.440	0.590	1.210	0.23	
v_g^p	3.50	6.500	2.500	2.000	3.690	5.6
v_s^p	9.00	12.000	6.200	3.800	5.800	10.09
v_s^m					0.530	
Minus-end stationary						
$\bar{l}$ (μm)	−15.12	13.55	−11.47	3.27	7.89	8.58
τ (min)	−6.46	3.83	−7.38	4.47	5.26	5.51
Minus-end $v_s^m = 0.53$						
$\bar{l}$ (μm)	−21.46	9.49	−49.67	1.74	5.20	8.58
τ (min)	−10.18	2.79	−37.03	2.81	3.75	5.51

The mean length $\bar{l}$ and mean lifetime τ in the absence of interactions or cell boundaries are computed using Eqs. 3–10 in Supplemental Material. The minus-end shrinking velocity is taken from the average shrinking velocity, including pauses, in Shaw et al. (2003). Because $\bar{l}$ and τ consider only the effects of dynamic instability, they should be thought of as characteristic scales that are perturbed by MT–MT interactions and the action of MAPs.

[a] Wild type.

a distance of $\delta = 25$ nm from the barrier MT in agreement with electron microscopy of cross-linking due to MAP65 (Chan *et al.*, 1999).

We consider two modes of MT nucleation. The first is independent of the extant MT array. MTs of zero initial length and uniform random orientation are inserted randomly into the cortex, at rate k_0 in micrometers^{-2} minute^{-1}. The second is MT-dependent nucleation, where new MTs are nucleated off extant MTs. The rate of MT-dependent nucleation will depend upon both the length of existing polymer and the number of available γ-TuRC in the cytoplasm (Murata *et al.*, 2005). However, we assume the γ-TuRC is rate limiting and thus MT-dependent nucleation occurs at a constant rate k_1 in minutes^{-1}. Once the new MT is nucleated, its plus-end immediately begins dynamic instability, and if $v_s^m > 0$, the minus-end immediately begins shrinking. In reality, there is likely to be a delay before katanin severs the minus-end (Sedbrook and Kaloriti, 2008), but because an actual lag time is unknown, we assume this is negligible. Also, we find that a completely static minus-end only delays the onset of self-organization, suggesting the katanin delay would not change our results significantly.

There are physical details not explicitly included in the model, such as the mechanical properties of the MTs, the cortex and the anchors connecting them. We assume that anchors are sufficiently strong and densely distributed along MTs so that 1) the radius of curvature of the cortex is not mechanically significant and 2) the kink in an entrained MT remains in place even if the barrier MT is removed through depolymerization.

We simulate on a 10- by 10-μm domain, which is a typical size of a plant cell face in early interphase, with periodic boundary conditions in both directions, except where we explicitly explore the consequences of boundaries. All simulations are run for 1000 min. We use a Gillespie algorithm to simulate switching between MT states (competing Poisson processes with rates f_{ij}) and

constant growth and shrinkage velocities, resulting in a variable timestep on the order of $\Delta t = 10^{-3}$ min. To detect and resolve collisions, we use a fixed timestep of $\Delta t = 0.05$ min. All simulations were replicated ten times with different, random initial conditions. We use dynamic instability parameters from Table 1, and, unless otherwise noted, other parameters from Table 2.

There are several ways to measure how well-oriented an array is. A common qualitative approach is to plot a histogram of MT angles defined so that the dominant direction is either 0 or 90° (Himmelspach *et al.*, 2003; Ambrose and Wasteneys, 2008). If the angle distribution is unimodal, its SD serves as a quantitative measure of orientation. As an extension of this, the distribution can be weighted by length, i.e., the angles of longer MTs count for more in the histogram.

More generally, Baulin *et al.* (2007) define an order parameter $0 < S_l < 1$ based on an angular cost function, weighted by l_i^2, where l_i is the length of each MT. Here, we define a slightly modified version of their order parameter, $S = \Sigma_i l_i (\cos^2(\theta_i - \Omega) - \sin^2(\theta_i - \Omega))/\Sigma_i l_i$, where θ_i is the angle of each straight MT segment and Ω is the dominant angle. Heuristically, S represents the relative difference between the projected polymer length in the dominant direction and the projected polymer length in its perpendicular direction.

RESULTS

Collision-induced Catastrophe Does Not Lead to Ordering for Physiological Kinetic Parameters

With parameters as given in Tables 1 and 2, CIC did not lead to any ordering. Instead, they lead to sparse arrays

Table 2. Parameters used in the model in addition to the dynamic instability parameters in Table 1

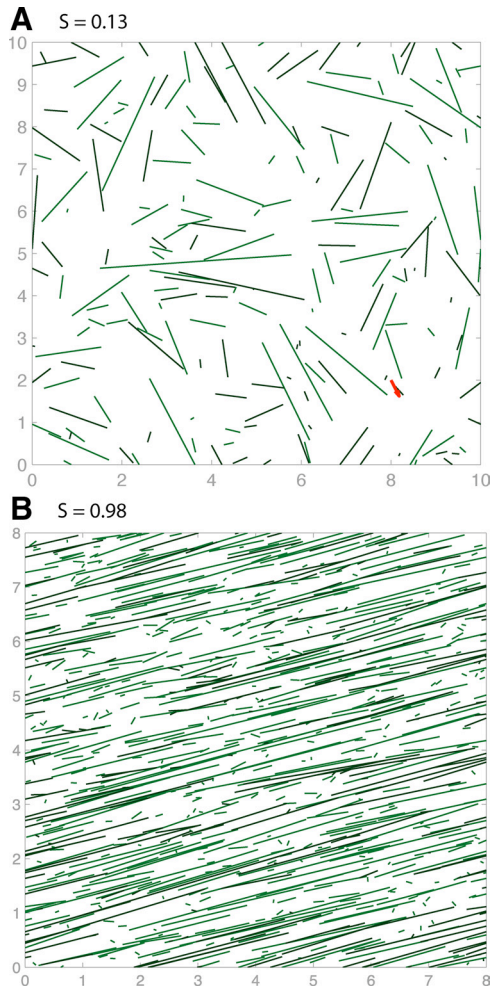| Parameter	Meaning	Value	Reference
θ_Z	Critical entrainment angle	40°, 60°	Ambrose and Wasteneys (2008), Dixit and Cyr (2004)
θ_{nuc}	Branched nucleation angle	40°	Murata *et al.* (2005)
k_0	Background nucleation rate	10 μm^{-2} min^{-1}	Estimated
k_1	MT-dependent nucleation rate	10^3 min^{-1}	Estimated
p_{cat}	Probability of catastrophe upon steep collision	0.09–0.6	Wightman and Turner (2007), Dixit and Cyr (2004)
p_{zip}	Probability of entrainment upon shallow collision	≈1	Dixit and Cyr (2004)
δ	Spacing between bundled MTs	25 nm	Chan *et al.* (1999)

Figure 1. Simulation snapshots at $t = 60$ min with collision-induced catastrophe only, using parameters from wild type at 31°C (Kawamura and Wasteneys 2008) (A) and collision-induced pauses, using the single-state model of Baulin *et al.* (2007) (B).

shown in Figure 1A. For high values of $p_{cat} = 0.9$ (shown in the figure), the MTs were too short in length and lifetime for orientation to emerge, whereas for low values of p_{cat} 0.1, they simply did not interact enough. Intermediate values of p_{cat} also failed to organize. However, Baulin *et al.* (2007) report that pause-inducing collisions alone are enough to give rise to an oriented array, a result we confirm with our simulations (see Figure 1B and Supplemental Movies S1 and S2). In the Supplemental Material, we show that the pause-inducing collision model is a limiting case of the catastrophe-inducing collision model. After conducting a random sweep of 10^3 kinetic parameter sets, we conclude that CIC only leads to self-organization in the limit where the shrinkage rate and catastrophe rate are approximately 0 ($v_s^p f_{gs} \approx 0$) and the rescue rate is much larger than the catastrophe rate ($f_{sg} \gg f_{gs}$), consistent with Baulin *et al.* (2007).

Plus-End Entrainment, with or without CIC, Results in an Ordered Array

Simulations that include entrainment gave rise to significant order parameters within the first 60 min. In Figure 2, we display snapshots from the simulations for the four kinetic

parameter sets taken from Kawamura and Wasteneys (2008) for plus-end dynamics and the average v_s^m from Shaw *et al.* (2003). In Figure 2, A–C, a single dominant direction is evident with patches of deviation present. The dominant direction (red arrows) is uniformly random (data not shown) across simulations and persists for at least 10^3 min.

The time course of some of these simulations are shown in Supplemental Movies S3–S7. Initially, several locally ordered domains emerge, grow and shrink (but never rotate, as reported in Chan *et al.* (2007)). By 10^3 min, typically a single orientation dominates. However, sometimes the cortex is divided into two domains with distinct dominant orientations. These directions were never observed to differ by more than the critical entrainment angle θ_Z. It remains possible that one of these domains becomes globally dominant on time scales much larger than 10^3 min.

In Figure 3, A and B, we show time series from 10 runs with wild-type 31°C parameters (blue curves). The mean lengths increase slowly. After $\sim 10^3$ min, in each simulation, the mean MT length converges to a value below $\bar{l}$, the predicted mean length in the absence of interaction (Table 1 and Eq. 8 in Supplemental Material). For comparison, single cortical MTs have been reported to be 2–4 μm when measured by transmission electron microscopy (Hardham, 1978). The number of MTs converges quickly to roughly 10^3 (data not shown). Note that the steady-state number of MTs depended on k_0, and we chose $k_0 = 10$ μm^{-2} min^{-1} to give $\sim 10^3$ MTs.

Using S as our measure of order, we conclude that plus-end entrainment does give rise to order. This order emerges with a time scale $< 10^2$ min (Figure 3B), in agreement with the observed time-to-order in vivo (Wasteneys and Williamson, 1989a). The full orientational distribution is shown in Figure 3C. Notably, without CIC in the simulations (i.e., $p_{cat} = 0$) ordering still emerged, see Figure 5A. Ordering also occurred using parameters from Shaw *et al.* (2003) and for the two-state model using parameters from Dixit and Cyr (2004) (data not shown).

With Kinetic Parameters Taken from the mor1-1 Mutant at 31°C, Ordered Arrays Do Not Form

In simulations of the *mor1-1* mutant at 31°C, the MTs were short and therefore much lower in total polymer density. From Figure 4A, we see their average length is 0.5 μm, roughly one sixth of their mean free length in the absence of interactions. Reducing the nucleation rate increased their mean length slightly but still did not allow for ordering.

Static Minus-Ends Delay, but Do Not Prevent, Array Organization

Although three-state dynamic instability of MT plus-ends has been reported extensively (Shaw *et al.*, 2003; Dixit and Cyr, 2004; Kawamura and Wasteneys, 2008), the hybrid treadmilling has been reported less often (Shaw *et al.*, 2003). To explore the consequences of a freely depolymerizing minus-end, we ran simulations with static minus-ends ($v_s^m = 0$).

A typical array arising from $v_s^m = 0$ is qualitatively similar to the arrays in Figure 2B, the equivalent runs with $v_s^m = 0.53$ μm/min. The order parameter S after 10^2 min is, on average, also comparable (0.9 and 0.8 for $v_s^m = 0.53$ μm/min and $v_s^m = 0$, respectively). However, static minus-ends seemed to delay the onset of self-organization. In Figure 3B, we show the order parameter's time evolution for both $v_s^m = 0.53$ μm/min (blue curves) and $v_s^m = 0$ (green curves). Although the
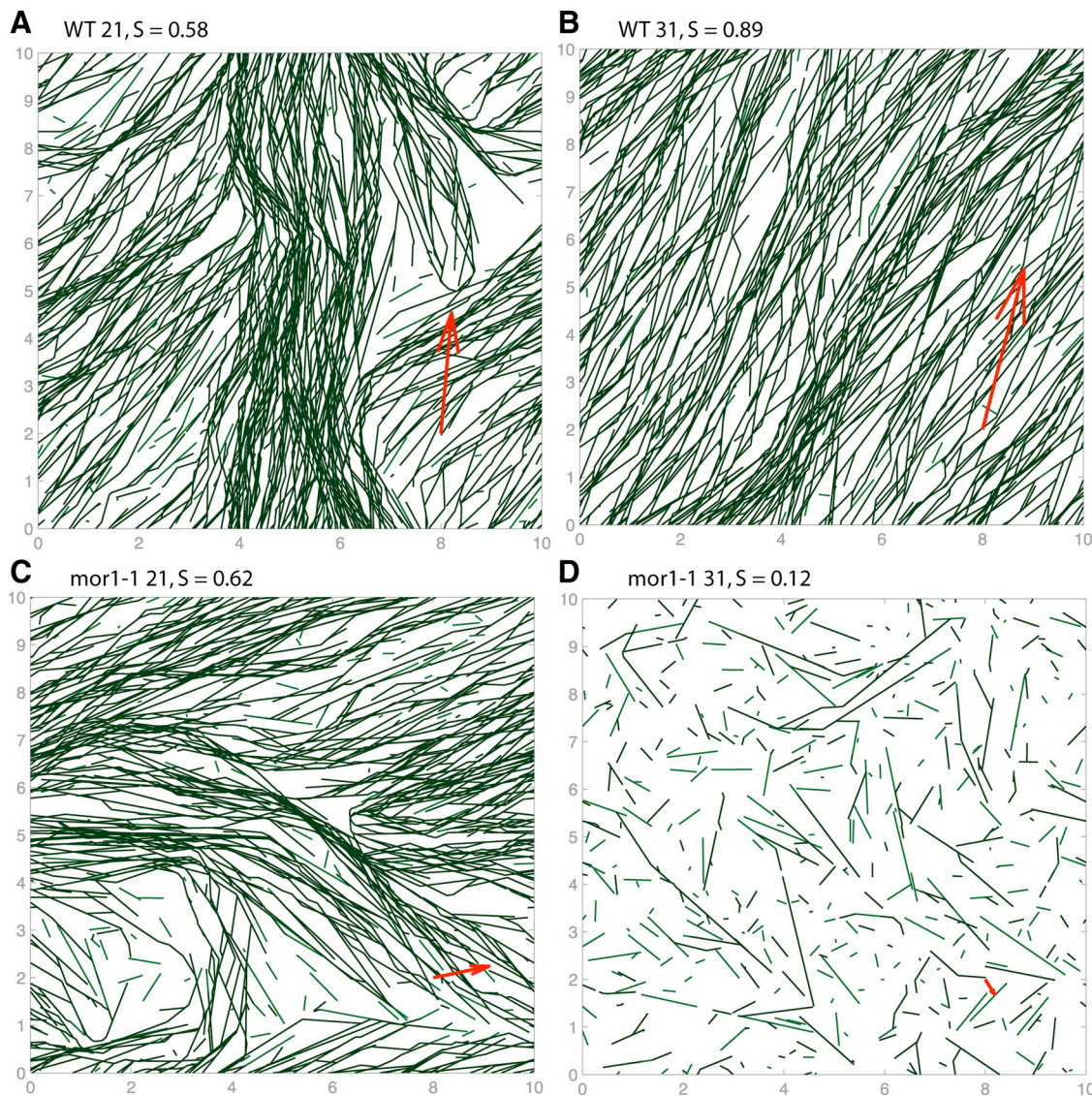
A WT 21, S = 0.58

B WT 31, S = 0.89

C mor1-1 21, S = 0.62

D mor1-1 31, S = 0.12

Figure 2. Collision-induced catastrophe at steep angles (>40°) and entrainment at shallow angles (<40°) for four sets of kinetic parameters from Kawamura and Wasteneys (2008) and continuously depolymerizing minus-end (Shaw *et al.*, 2003). The top (A and B) and bottom (C and D) rows are wild-type and *mor1-1* kinetic parameters, respectively, and the left (A and C) and right (B and D) are at 21 and 31°C, respectively. New MTs are inserted randomly at a rate of $k_0 = 10 \ \mu m^{-2} \ min^{-1}$. The boundaries are periodic in both directions. After 60 min, order emerges in local domains in all cases except *mor1-1* at 31°C. The direction of the red arrow indicates the dominant direction of the MT array, whereas their lengths are proportional to the order parameter.

simulation with a shrinking minus-end has reached its well-ordered steady-state (within 10% of its steady-state order parameter *S*) within 20 min, it takes the simulation with static minus-ends roughly 80 min, which is 4 times longer.

Static Minus-Ends Allow "mor1-1" to Self-Organize

The dynamics of the minus-ends affect the average length of MTs (Table 1) in that if minus-ends are static, the MTs grow slightly longer. In simulations with kinetic parameters from the *mor1-1* mutant at 31°C, we find that static minus-ends induce a change sufficient to allow for ordering. Time series data for this kinetic parameter set are shown in Figure 4, A and B. The order parameter in Figure 4B shows that the mutant with a depolymerizing minus-end does not organize (blue curve). With static minus ends, organization is rescued (green curve). In this case, however, self-organization still

takes longer than in simulations of wild-type plants with nonstatic minus ends.

Increasing the Critical Entrainment Angle Does Not Enhance, but Rather Delays, Array Organization

MTs in the *clasp-1* mutant described by Ambrose and Wasteneys (2008) entrain over a wider range of incident angles, with a mean entrainment angle roughly 11° larger than in wild type and demonstrate "hyperparallel" arrays, indicated by a smaller SD of MT orientations. To test whether a higher critical entrainment angle can explain the hyperparallel arrays, we ran simulations in which we increased the critical entrainment angle from $\theta_Z = 40°$ to $\theta_Z = 60°$, which is equivalent to increasing the mean entrainment angle by 10°.

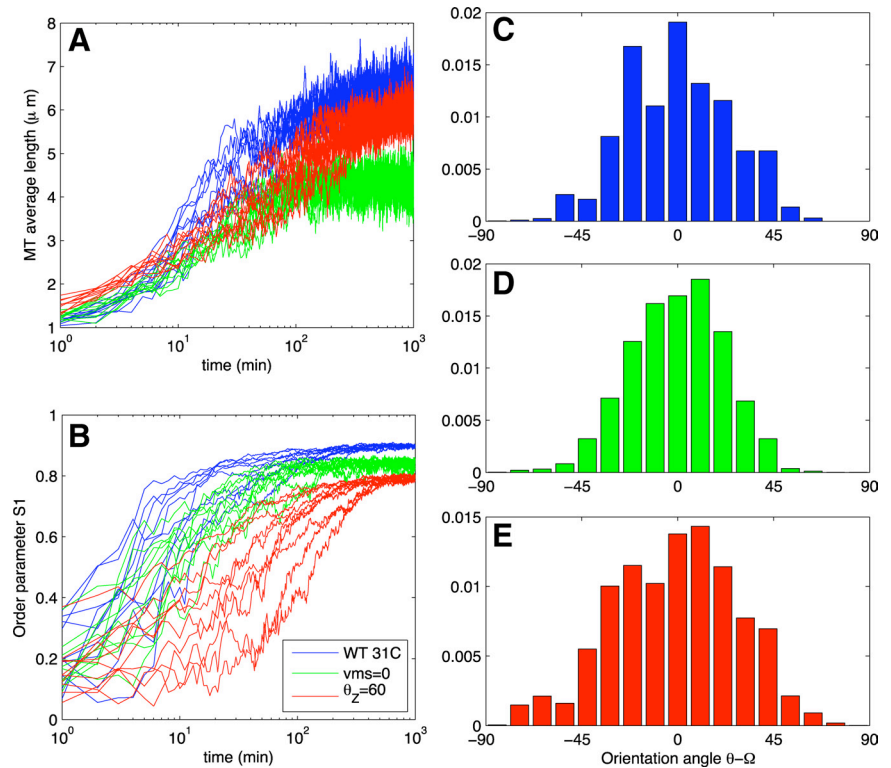Qualitatively, the resulting arrays seem indistinguishable from the corresponding array in Figure 1 (see Supplemental

Figure 3. Data from wild-type (WT) simulation runs. (A) Average length of an MT. (B) Order parameter S, given by the equation in *Materials and Methods* [a modified version of the Baulin *et al.* (2007) order parameter]. All simulations use kinetics from wild type at 31°C in Table 1. (C–E) Histograms from selected runs depicted in Figure 2. Blue curves in A and B and histogram in C have a depolymerizing minus end and a critical entrainment angle of $\theta_Z = 40°$. Green curves in A and B and histogram in D have a static minus-end ($v_s^p = 0$) with $\theta_Z = 40°$, and red curves in A and B and histogram in E have depolymerizing minus end with $\theta_Z = 60°$. Time series from 10 independent simulations are shown in each case.

Movie S8). However, examining the time course of the order parameter S reveals that the increased θ_Z delays and slightly reduces array ordering, similar to the case of static minus-ends. The time series of ordering is shown in red in Figure 3B, with a typical angle distribution in Figure 3E. This suggests that the *clasp-1* hyperparallel MT phenotype is dependent on another mechanism.

MT-dependent Branched Nucleation Leads to Unrealistic Array Structures

Up to this point, all MT nucleation has been assumed to occur uniformly in space and at random angles, referred to here as background nucleation. To explore the reports of MT-dependent branched nucleation, we ran simulations
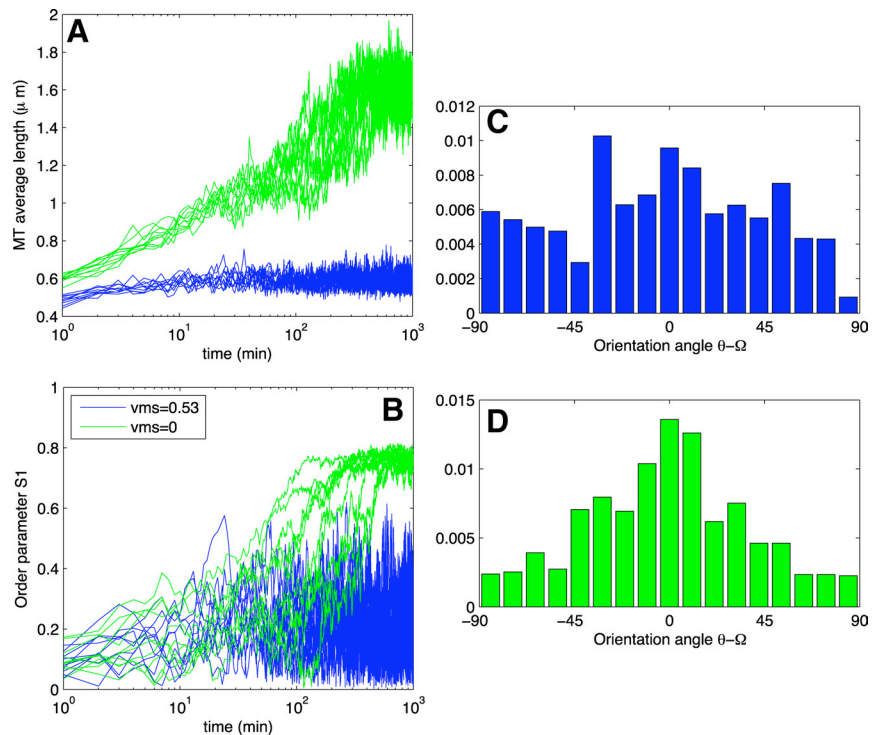

Figure 4. Data from simulations of the *mor1-1* mutant. (A) Average length of an MT. (B) Order parameter S, given by the equation in *Materials and Methods* [a modified version of the Baulin *et al.* (2007) order parameter]. All simulations use kinetics from *mor1-1* at 31°C in Table 1. Blue curves in A and B and histogram in C have a depolymerizing minus end, whereas green curves and histogram in D have a static minus-end ($v_s^p = 0$).
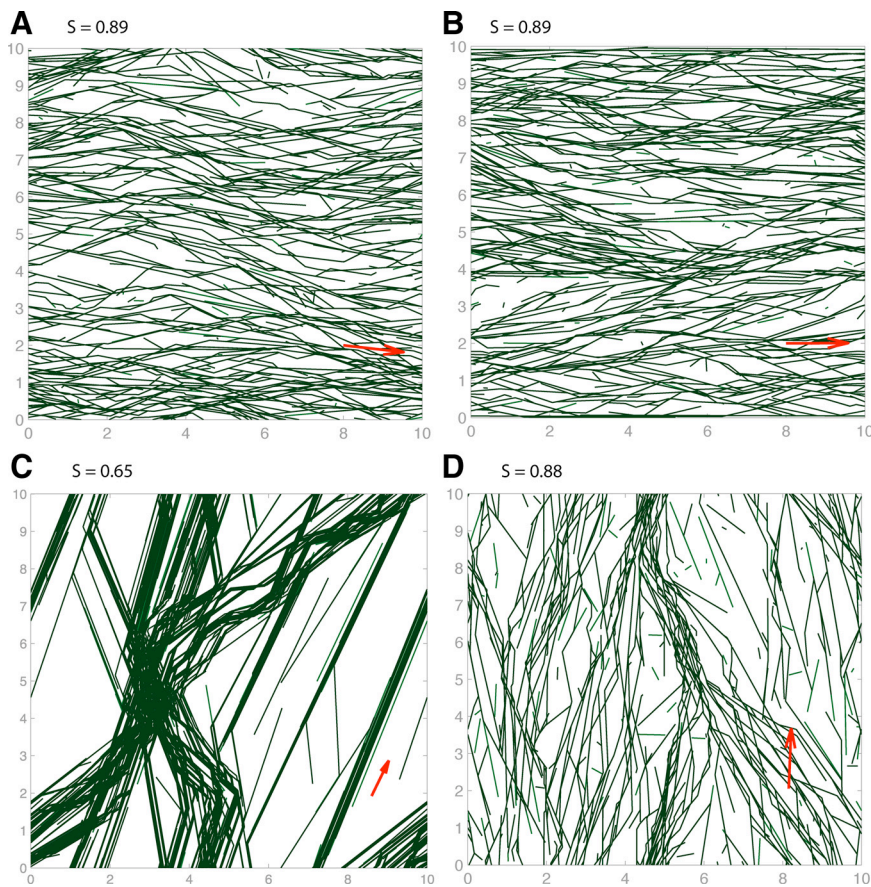
Figure 5. Simulation snapshots at $t = 60$ min using kinetic parameters from wild type at 31°C. (A) Entrainment at shallow angles (<40°) and no collision-induced catastrophe ($p_{cat} = 0$). (B) A biased, transverse dominant angle that arises if two edges (here, the top and bottom) induce catastrophe. This provides a possible mechanism for selecting a direction transverse to the cell elongation axis. (C) Sparse array that results if all nucleation is branched MT-dependent nucleation. (D) Moderately sparse array arising from a combination of MT-dependent and MT-independent nucleation.

without background nucleation ($k_0 = 0$) and nonzero MT-dependent nucleation rate $k_1 = 10^3$ min^{-1}.

These simulations always resulted in arrays with a distinct structure reminiscent of shattered glass. As with background nucleation, one or a few dominant angles emerged locally at early times, the domains grew or shrank, and often one direction dominated globally. However, the arrays were always sparse with large gaps free of persisting MTs. A typical snapshot is shown in Figure 5C. Time courses of typical simulations are shown in Supplemental Movies S9 and S10.

Although MT-dependent branch nucleation alone leads to an unrealistic array organization, this does not necessarily mean it is not important. We ran simulations with a combination of MT-dependent and MT-independent nucleation. As MT-independent nucleation is reduced, the arrays seemed more and more sparse. A simulation with a combination of nucleation types, $k_1 = 500$ min^{-1} and $k_0 = 5$ min^{-1} μm^{-2}, is shown in Figure 5D.

Catastrophe-inducing Boundaries Are Enough to Bias the Dominant Orientation

Up to now, all simulations described were carried out on a square cortex with periodicity in both directions. That is, an MT that disappears off any edge appears from the opposite edge. When a dominant angle emerges in our simulations, it is uniformly random. In diffusely elongating plant cells, the dominant angle is transverse to the direction of elongation, indicating that there must be a symmetry-breaking mechanism that signals a preferred orientation to the MTs. One candidate for this mechanism is interaction with the apical and basal poles of the plant cell (Ehrhardt and Shaw, 2006).

Real cells have distinct faces. Side walls may allow MTs oriented transverse to the elongation axis to continue growing indefinitely, unperturbed by boundaries between faces. In the longitudinal direction, MTs can treadmill onto the cross walls but rarely do (Collings and Wasteneys, 2005). It has been suggested that the boundaries of the poles inhibit MT growth, either sterically or through MAP activity (Ehrhardt and Shaw, 2006). We represent this interaction by imposing catastrophe on any MT that collides with the top or bottom of the cylinder.

We find that this catastrophe-inducing boundary effect is enough to cause selection of the transverse angle as the dominant orientation. Snapshots from these simulations are shown in Figure 5B. At $t = 60$ min, not all nontransversely oriented patches disappear, yet the dominant transverse angle always persists.

In fact, even in the complete absence of MT–MT interactions, catastrophe-inducing boundaries at the cross-walls will lead to a certain amount of ordering. MTs transverse to the elongation axis can treadmill indefinitely, whereas those parallel to the elongation axis will quickly encounter a boundary. The ordering of MTs is therefore strongest near the cross walls and decays toward the mid-cell over a distance of roughly the mean length in the absence of interaction (see Supplemental Material for details). MT–MT interaction allows this boundary-induced orientation to propagate further into the mid-cell cortex. We also found that the introduction of catastrophe-inducing boundaries does not induce ordering in the CIC-only model described above.

DISCUSSION

Recent genetic and pharmacological experiments on cortical MTs in plants have given rise to a model for the self-organization of these MTs into a parallel array. Here, we have presented the results of large-scale simulations of a quantitative implementation of this model. We find that self-organization into a parallel array can arise from a combination of MT dynamic instability, plus-end entrainment, and, in certain cases, CIC. The arrays that arise in our simulations seem qualitatively similar to the arrays in plant cells, including the local domains of orientation that are similar to the patchwork patterns in maturing *Chara* cells (Wasteneys *et al.*, 1993) and the outer epidermis of *Arabidopsis* hypocotyl cells (Chan *et al.*, 2007). In addition to recapitulating wild-type behavior, our model also agrees with mutant studies (Kawamura and Wasteneys, 2008).

It has been proposed that CIC can explain ordering. Our results show that CIC is neither necessary nor sufficient for ordering when physiologically reasonable dynamic instability parameters are used. Previous modeling efforts have focused on the role of CIC in the emergence of order. Dixit and Cyr (2004) showed that CIC in combination with plus-end entrainment leads to ordering. In light of our results, we suggest ordering in their model arises due to entrainment rather than CIC. The model of Baulin *et al.* (2007) corresponds to a limit in which the growth rate dominates the shrinkage rate, and the rescue frequency dominates the catastrophe frequency. This model fails to self-organize when extended to a regime that matches reported kinetic parameters (Shaw *et al.*, 2003; Dixit and Cyr, 2004; Kawamura and Wasteneys, 2008).

Plus-end entrainment with branched MT-dependent nucleation gives rise to an oriented array that seems sparse because areas of low MT content have no candidate nucleation sites, whereas areas of high MT content have many. From this, we conclude that exclusive MT-dependent branched nucleation leads to unrealistic array structures. Free nucleation seems to be necessary to explain the dispersed arrays seen in vivo. This seems to contradict the hypothesis that branched nucleation helps to disperse the array throughout the cortex (Wasteneys and Ambrose, 2009), but is consistent with the observation that during recovery from drug-induced disassembly, the initial transverse order of freely nucleated MTs is progressively lost when most subsequent MTs are produced by branch-form nucleation (Wasteneys and Williamson, 1989a). Although MT-dependent branch-form nucleation alone leads to unrealistic arrays, this does not suggest that it does not occur. As proposed by Wasteneys and Ambrose (2009), it may be specifically promoted under conditions where it is beneficial to change the predominant orientation of MTs. Recent improvements in live cell imaging has enabled the detection of microtubule-dependent nucleation that is parallel to the parent MT (see figure 1C in Ambrose and Wasteneys 2008) and this alternative form of MT-dependent nucleation might prove to be much more common than previously thought (Wasteneys and Ambrose 2009).

We find that increasing the critical entrainment angle does not enhance the array order. In fact, order is reduced slightly and delayed. This conflicts with recent experiments in which Ambrose and Wasteneys (2008) observed "hyperparallel" arrays in the *clasp-1* mutant. This suggests that the CLASP protein affects array organization through more than simply modulating the critical entrainment angle.

Two of the phenomena we neglect in our simulations are increased MT stability through bundling, and severing after crossover. MTs within bundles remain dynamic, however, with slightly modified kinetic parameters (Van Damme *et al.*, 2004). It is unknown whether this effect arises simply through the reduced collision frequency or whether it is important for MT array organization. MT severing at sites of existing crossovers, possibly mediated by katanin, also has been reported (Wightman and Turner, 2007); however, this occurs rarely as severing of elongated MTs is rare (Shaw *et al.*, 2003).

Three novel predictions arise from this work. First, if the transverse dominant direction is selected by catastrophe-inducing boundaries at the top and bottom edges of the cell, then the time to order will increase as the cell length increases, as it takes longer for the signal to propagate inward.

The other two predictions demonstrate the paradoxical influence of static minus ends. First, if minus-ends do not become mobile in wild type (e.g., in a katanin knockout), we predict ordering to take fourfold longer. Second, we predict that a similar perturbation of the *mor1-1* 31°C mutant rescues ordering.

This last set of predictions illustrates one of the values of computational modeling. The subtle influence of static as opposed to mobile minus-ends, which in one case promotes and in the other inhibits organization, is essentially impossible to tease out without recourse to computational techniques.

REFERENCES

Ambrose, J. C., and Wasteneys, G. O. (2008). CLASP modulates microtubule-cortex interaction during self-organization of acentrosomal microtubules. Mol. Biol. Cell *19*, 4730–4737.

Baulin, V. A., Marques, C. M., and Thalmann, F. (2007). Collision induced spatial organization of microtubules. Biophys. Chem. *128*, 231–244.

Brouhard, G. J., Stear, J. H., Noetzel, T. L., Al-Bassam, J., Kinoshita, K., Harrison, S. C., Howard, J., and Hyman, A. A. (2008). XMAP215 is a processive microtubule polymerase. Cell *132*, 79–88.

Burbank, K. S., Mitchison, T. J., and Fisher, D. S. (2007). Slide-and-cluster models for spindle assembly. Curr. Biol. *17*, 1373–1383.

Chan, J., Calder, G., Fox, S., and Lloyd, C. (2007). Cortical microtubule arrays undergo rotary movements in *Arabidopsis* hypocotyl epidermal cells. Nat. Cell Biol. *9*, 171–175.

Chan, J., Calder, G. M., Doonan, J. H., and Lloyd, C. W. (2003). EB1 reveals mobile microtubule nucleation sites in *Arabidopsis*. Nat. Cell Biol. *5*, 967–971.

Chan, J., Jensen, C. G., Jensen, L.C.W., Bush, M., and Lloyd, C. W. (1999). The 65-kDa carrot microtubule-associated protein forms regularly arranged filamentous cross-bridges between microtubules. Proc. Natl. Acad. Sci. USA *96*, 14931–14936.

Collings, D., and Wasteneys, G. (2005). Actin microfilament and microtubule distribution patterns in the expanding root of *Arabidopsis thaliana*. Can. J. Bot. *83*, 579–590.

Dhonukshe, P., Laxalt, A. M., Goedhart, J., Gadella, T.W.J., and Munnik, T. (2003). Phospholipase D activation correlates with microtubule reorganization in living plant cells. Plant Cell *15*, 2666.

Dixit, R., and Cyr, R. (2004). Encounters between dynamic cortical microtubules promote ordering of the cortical array through angle-dependent modifications of microtubule behavior. Plant Cell *16*, 3274–3284.

Dogterom, M., and Leibler, S. (1993). Physical aspects of the growth and regulation of microtubule structures. Phys. Rev. Lett. *70*, 1347–1350.

Ehrhardt, D. W., and Shaw, S. L. (2006). Microtubule dynamics and organization in the plant cortical array. Annu. Rev. Plant Biol. *57*, 859–875.

Gardner, M. K., Hunt, A. J., Goodson, H. V., and Odde, D. J. (2008). Microtubule assembly dynamics: new insights at the nanoscale. Curr. Opin. Cell Biol. *20*, 64–70.

Grill, S. W., and Hyman, A. A. (2005). Spindle positioning by cortical pulling forces. Dev. Cell *8*, 461–465.

Groen, A. C., Maresca, T. J., Gatlin, J. C., Salmon, E. D., and Mitchison, T. J. (2009). Functional overlap of microtubule assembly factors in chromatin-promoted spindle assembly. Mol. Biol. Cell *20*, 2766.

Hardham, A. (1978). Structure of cortical microtubule arrays in plant cells. J. Cell Biol. *77*, 14–34.

Hashimoto, T., and Kato, T. (2006). Cortical control of plant microtubules. Curr. Opin. Plant Biol. *9*, 5–11.

Himmelspach, R., Williamson, R. E., and Wasteneys, G. O. (2003). Cellulose microfibril alignment recovers from DCB-induced disruption despite microtubule disorganization. Plant J. *36*, 565.

Kawamura, E., and Wasteneys, G. O. (2008). MOR1, the *Arabidopsis thaliana* homologue of *Xenopus* MAP215, promotes rapid growth and shrinkage, and suppresses the pausing of microtubules in vivo. J. Cell Sci. *121*, 4114.

Malikov, V., Cytrynbaum, E. N., Kashina, A., Mogilner, A., and Rodionov, V. (2005). Centering of a radial microtubule array by translocation along microtubules spontaneously nucleated in the cytoplasm. Nat. Cell Biol. *7*, 1213–1218.

Mitchison, T., and Kirschner, M. (1984). Dynamic instability in microtubule growth. Nature *312*, 237–242.

Murata, T., Sonobe, S., Baskin, T. I., Hyodo, S., Hasezawa, S., Nagata, T., Horio, T., and Hasebe, M. (2005). Microtubule-dependent microtubule nucleation based on recruitment of big gamma-tubulin in higher plants. Nat. Cell Biol. *7*, 961–968.

Pinot, M., Chesnel, F., Kubiak, J. Z., Arnal, I., Nedelec, F. J., and Gueroui, Z. (2009). Effects of confinement on the self-organization of microtubules and motors. Curr. Biol. *19*, 954–960.

Rubin, R. J. (1988). Mean lifetime of microtubules attached to nucleating sites. Proc. Natl. Acad. Sci. USA *85*, 446–448.

Sedbrook, J. C., and Kaloriti, D. (2008). Microtubules, MAPs and plant directional cell expansion. Trends Plant Sci. *13*, 303–310.

Shaw, S. L., Kamyar, R., and Ehrhardt, D. W. (2003). Sustained microtubule treadmilling in *Arabidopsis* cortical arrays. Science *300*, 1715–1718.

Surrey, T., Nedelec, F., Leibler, S., and Karsenti, E. (2001). Physical properties determining self-organization of motors and microtubules. Science *292*, 1167–1171.

Van Damme, D., Van Poucke, K., Boutant, E., Ritzenthaler, C., Inze, D., and Geelen, D. (2004). In vivo dynamics and differential microtubule-binding activities of MAP65 proteins 1. Plant Physiol. *136*, 3956–3967.

Wasteneys, G., Gunning, B., and Hepler, P. (1993). Microinjection of fluorescent brain tubulin reveals dynamic properties of cortical microtubules in living plant-cells. Cell Motil. Cytoskeleton *24*, 205–213.

Wasteneys, G. O. (2002). Microtubule organization in the green kingdom: chaos or self-order? J. Cell Sci. *115*, 1345–1354.

Wasteneys, G. O. (2004). Progress in understanding the role of microtubules in plant cells. Curr. Opin. Plant Biol. *7*, 651–660.

Wasteneys, G. O., and Ambrose, J. C. (2009). Spatial organization of plant cortical microtubules: close encounters of the 2D kind. Trends Cell Biol. *19*, 62–71.

Wasteneys, G. O., and Fujita, M. (2006). Establishing and maintaining axial growth: wall mechanical properties and the cytoskeleton. J. Plant Res. *119*, 5–10.

Wasteneys, G. O., and Williamson, R. E. (1989a). Reassembly of microtubules in *Nitella tasmanica*: quantitative analysis of assembly and orientation. Eur. J. Cell Biol. *50*, 76–83.

Wasteneys, G. O., and Williamson, R. E. (1989b). Reassembly of microtubules in *Nitella tasmanica*: assembly of cortical microtubules in branching clusters and its relevance to steady-state microtubule assembly. J. Cell Sci. *93*, 705–714.

Whittington, A., Vugrek, O., Wei, K., Hasenbein, N., Sugimoto, K., Rashbrooke, M., and Wasteneys, G. (2001). MOR1 is essential for organizing cortical microtubules in plants. Nature *411*, 610–613.

Wightman, R., and Turner, S. R. (2007). Severing at sites of microtubule crossover contributes to microtubule alignment in cortical arrays. Plant J. *52*, 742.

Wollman, R., Cytrynbaum, E., Jones, J., Meyer, T., Scholey, J., and Mogilner, A. (2005). Efficient chromosome capture requires a bias in the 'search-and-capture' process during mitotic-spindle assembly. Curr. Biol. *15*, 828–832.